

RXTE OBSERVATIONS OF HERCULES X-1 DURING THE 1998 JULY SHORT HIGH STATE

MARTIN STILL¹

NASA/Goddard Space Flight Center, Code 662, Greenbelt, MD 20771; and School of Physics and Astronomy, University of St. Andrews, North Haugh, St. Andrews, Fife KY16 9SS, Scotland, UK

KIERAN O'BRIEN

School of Physics and Astronomy, University of St. Andrews, North Haugh, St. Andrews, Fife KY16 9SS, Scotland, UK

KEITH HORNE

School of Physics and Astronomy, University of St. Andrews, North Haugh, St. Andrews, Fife KY16 9SS, Scotland, UK; and Department of Astronomy, University of Texas at Austin, RLM 15.308, Austin, TX 78712

DANNY HUDSON² AND BRAM BOROSON

NASA/Goddard Space Flight Center, Code 662, Greenbelt, MD 20771

SAEQA DIL VRTILEK

High Energy Astrophysics Division, Harvard-Smithsonian Center for Astrophysics, 60 Garden Street, Cambridge, MA 02138

HANNAH QUAINIRELL

Department of Physics and Astronomy, Open University, Walton Hall, Milton Keynes MK7 6AA, UK

AND

HAUKE FIEDLER

Institut für Astronomie und Astrophysik, Ludwig-Maximilians-Universität, Scheinerstrasse 1, D-81679 München, Germany

Received 2000 August 7; accepted 2001 February 7

ABSTRACT

We present *RXTE* monitoring of the eclipsing X-ray binary Hercules X-1 conducted over the short high state of 1998 July. This was one of the last major short high states before the source entered an anomalous low state of activity. A comparison with previous epochs finds no evidence for special behavior during these observations. We determine orbital and pulsar spin periods to facilitate measurements of \dot{P}_{spin} and \dot{P}_{orb} during the subsequent anomalous low state and the next epoch of high-state activity. Spectrally, the decay of the short high state and concurrent pre-eclipse dips are consistent with obscuration of a central X-ray source by a cloud of nonuniform column density. The standard model of a warped accretion disk of finite vertical scale height fits the characteristics of this absorber well. Pre-eclipse dips have durations a factor of a few longer than the characteristic durations of dips during main high states. Pulse profile structure increases in complexity toward the tail of the short high state, suggesting changes in accretion curtain geometry.

Subject headings: accretion, accretion disks — binaries: close — binaries: eclipsing — stars: individual (Hercules X-1) — stars: neutron — X-rays: stars

On-line material: color figures

1. INTRODUCTION

Her X-1 (Tananbaum et al. 1972) is an eclipsing X-ray binary containing a pulsar of $1.4 M_{\odot}$ and an A7 stellar companion of $2.2 M_{\odot}$ (Middleditch & Nelson 1976; Reynolds et al. 1997). The system displays behavior on four separate periodicities—the pulsar spin period (1.24 s), the binary orbit (1.7 days), a super period of 35 days, which results from a retrograde-precessing, warped accretion disk, and a beat between the precessional and orbital periods of 1.62 days. The warp engine is poorly understood but is likely to be a combination of both radiationally and tidally driven precession (Papaloizou & Terquem 1995; Pringle 1996).

In X-rays the 35 day supercycle results in two phases of strong X-ray activity per cycle (Giacconi et al. 1973; Scott & Leahy 1999). The main high state has a rapid turn-on over ~ 90 m and decays over ~ 10 days. A low state where flux remains at 3%–5% of the high-state level follows for the next ~ 10 days, succeeded by a second short high state,

lasting ~ 5 days, with flux peaking at $\sim 30\%$ of the main-high-state maximum. A further low state completes the cycle and extends over the next ~ 10 days. UV, optical, and infrared wavelengths are dominated by X-ray emission reprocessed over the inner face of the companion star. There is no high-low state switching in these wavebands because the pulsar is always visible to a large fraction of the companion star's surface; however, the accretion disk casts a shadow over the stellar photosphere, whose terminator migrates on the precession timescale. Consequently, the supercycle is also observed at UV, optical, and infrared energies (Gerend & Boynton 1976).

The 35 day clock has remained quasi-coherent since its discovery, although there have been two recorded occasions when the clock has missed several consecutive turn-ons (Parmar et al. 1985, 1999) and one occasion when the X-ray flux during main high states was significantly reduced (Vrtilek et al. 1994). The cause of these anomalous low states is not clear, but they probably result from changes in the state of the accretion disk, either through an increase in vertical scale height or modifications to the disk warp. However, the relatively constant level of UV and optical flux during these states suggests that accretion does not turn off altogether.

¹ Universities Space Research Association.

² Joint Center for Astrophysics, University of Maryland, Baltimore County, MD 21250.

During the spring of 1999, Her X-1 entered its latest anomalous low state and remained there until the fall of 2000. Figure 1 presents the long-term light curve of Her X-1, sampled once per day over the energy band 2–10 keV, as obtained by the *RXTE* All-Sky Monitor (ASM) on board *RXTE* (courtesy of the ASM team; Levine et al. 1996). After MJD 51,200 there are two weak main high states before the onset of the anomalous low state. The data presented in this paper were taken at MJD 51,000, which appears to be a normal short high state. However, all subsequent short high states appear either to be absent or weak within the sensitivity limits of the ASM. This suggests that a precursor to the anomalous low state may be a weakening of short high states beginning some 200 days before the main high states vanish. This would have consequences for the timescale of mass transfer variability in the system and the dynamical reaction time of the disk warp to mass transfer rate onto the neutron star.

The same short high state was simultaneously observed with *BeppoSAX*. Oosterbroek et al. (2000) present data obtained with the Low-Energy Concentrator Spectrometer (LECS; 0.1–10 keV) and the Medium-Energy Concentrator Spectrometer (MECS; 1.8–10 keV) experiments over four orbital cycles. They discern long-duration, energy-dependent dips in the light curve as well as model spectra as composites of power-law, blackbody, and Fe line components, provide energy-resolved pulse profiles, and fit pulse-phased spectral models to the data. The 100 eV blackbody component displays pulses that are out of phase with the power-law component. It is believed to originate from the inner regions of the accretion disk.

Oosterbroek et al. (2000) provide spectral models and spin-phased light curves for the least absorbed intervals of each orbit but do not follow the spectral or pulse profile evolution through dipping events. The larger collecting area of *RXTE* compared with *BeppoSAX* allows us to present pulse profiles and spectral fits through the dipping events and over an energy band harder than the *BeppoSAX* LECS and MECS instruments. In the following discussion we also search for any outstanding properties of this short high state that might signal the onset of any future anomalous low states and measure the pulsar orbital and spin periods to help enable the correct measurement of orbital and rotational changes during the low state. These data form part of a simultaneous multiwavelength campaign of Her X-1 (Borison et al. 2000a, 2000b; Still et al. 2001; Vrtilik et al. 2001; this paper) consisting of pointings from *RXTE*, the *Extreme Ultraviolet Explorer*, the *Hubble Space Telescope*

(*HST*), the 4.2 m William Herschel telescope on La Palma, and the 3.5 m Calar Alto telescope, Spain.

2. OBSERVATIONS

RXTE pointed at Her X-1 intermittently during 1998 July 9–13 (MJD 51,003.8–51,007.9), accumulating 70 ks of time-tagged events. Assuming the 35 day epoch is determined by (M. Kunz 2000, private communication)

$$T_{35} = \text{MJD } 50,041.0 + 34.85E_{35}, \quad (1)$$

where T_{35} corresponds to the X-ray turn-on of the main high state, and E_{35} is the cycle number, the precession phases sampled are $\phi_{35} = 0.63\text{--}0.74$. This range corresponds approximately to the range from the peak of a short high state to the end of the short high state (Scott & Leahy 1999).

Event reconstruction was performed using standard algorithms within FTOOLS Version 4.2. We analyze data from the Proportional Counter Array (PCA; Zhang et al. 1993), which consists of five identical Xe Proportional Counting Units (PCUs) with a combined effective area of 6500 cm². As well as the standard data formats, we employ two event analyzers in the GoodXenon event mode with 2 s readout. Time stamps are resolved to 1 μ s while employing the full 256 energy channels (1.8–101.0 keV during epoch 3). Response matrices from 1998 July 9 were obtained from the HEASARC archive.³ At various times 3–5 PCUs were active. Background estimates are derived from the very large event (VLE) model to account for cosmic events, internal particle generation, and South Atlantic Anomaly activation.⁴

3. LIGHT CURVES

Standard2 data from each visit were filtered to reject pointings closer than 10° to the Earth’s limb or off-axis by 0:02 or greater. Events were summed across pulse-height channels to provide a light curve in the energy range 2–28 keV with 100 s sampling and over all PCA layers and columns. This is presented in Figure 2 with hardness ratios of 5–8 keV/2–5 keV and 8–20 keV/5–8 keV. Background models have been subtracted and data scaled by the number of active PCUs.

X-ray count rates display a general trend of decline between the first and last visits, interrupted by dipping episodes. The event centered at MJD 51,004.7 is an eclipse of the X-ray source by the companion star. The same eclipse observed in the broad UV emission lines by *HST* provided constraints on the location of dynamic gas in the system (Borison et al. 2000a). We observe residual counting events at mideclipse with a weighted average rate of 1.0 ± 0.2 counts s⁻¹ PCU⁻¹, determined from visits 9 and 10. From time-dependent spectral fits to *GINGA* Large Area Counter (LAC) eclipse pointings, Choi et al. (1994a) and Leahy (1995) argue for an extended, ionized, scattering region around Her X-1 producing these residual photons from where the mideclipse fluxes were found to be variable by a factor of 7 from orbit to orbit. It was suggested that variability is related to the 35 day cycle, although no correlation

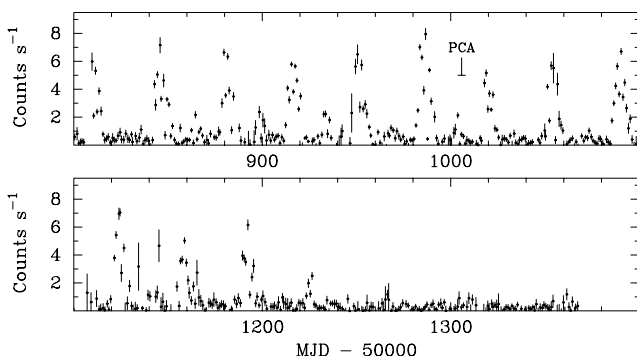


FIG. 1.—*RXTE* ASM light curve of Her X-1. The label “PCA” indicates the time and combined duration of the current short-high-state visits.

³ See <http://xte.gsfc.nasa.gov>.

⁴ See <http://lhe.gsfc.nasa.gov/stark/pca/pcabackest.html>.

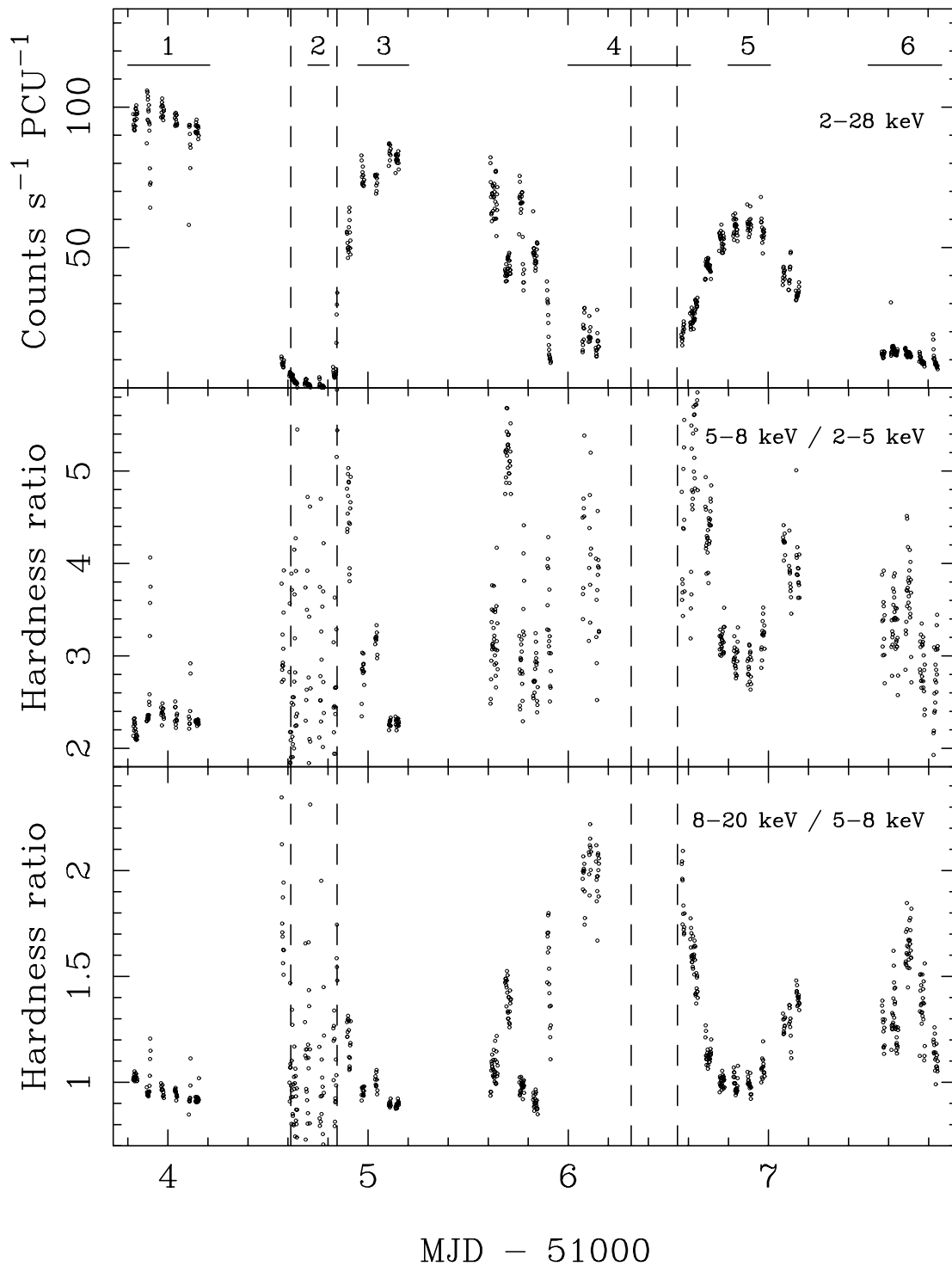


FIG. 2.—2–28 keV light curve of Her X-1, spanning approximately the peak of the short high state to its end. Dashed lines correspond to the beginning and end of X-ray eclipse. The lower panels display the hardness ratios between the bands 2–5, 5–8, and 8–20 keV. Data used to extract spin pulse profiles (§ 6) were taken from time sequences 1–6.

has been searched for. However, by folding spectral models of visits 9 and 10 (§ 4) through the response matrix of the LAC, we find these residual counts to be consistent with the *GINGA* detection of $2.1 \text{ counts s}^{-1}$ at $\phi_{35} = 0.67$.

Between MJD 51,005.8 and 51,006.8 we observe an extended dip with a duration of roughly half an orbital period. Although our sampling is not ideal, the data are

suggestive of dips with similar phasing and duration both preceding and following orbital cycles. This is confirmed by the more complete sampling of the contemporaneous *BeppoSAX* observations of Oosterbroek et al. (2000). Dip ingress occurs earlier each consecutive orbit, while the dip duration increases. Hardness ratios suggest that these are, at least partially, the result of photoelectric absorption,

although the dips remain strong features at energies greater than 10 keV. Both Shakura et al. (1998) and Scott & Leahy (1999) folded data from the *RXTE* ASM archive and found that short-high-state dips have significantly longer durations than main-high-state dips. The ASM shows that the width of these features is coherent from cycle to cycle over many years and therefore is not related to the impending X-ray low state. Long dip durations are probably the result of blending by numerous unresolved shorter events (Reynolds & Parmar 1995).

Crosa & Boynton (1980) determined that dip ingresses migrate linearly toward earlier orbital phases over each 35 day period, where the time between successive ingresses is 1.65 days. Although this is not exactly the beat between the 35 day and orbital cycles, Crosa & Boynton suggest that the dips are the result of periodic increases in the scale height of the outer accretion disk brought on by bursts of mass transfer as the L_1 point of the companion star sweeps through the X-ray shadow of the disk. The dip period is the sum of the beat period and the orbital timescale of structure in the outer disk traveling from the accretion stream impact point to the pulsar line of sight. It is difficult to see how this model incorporates dips of precession-coherent duration unless the accretion stream meets the disk at a radius that varies over the 35 day cycle. This would result in a range of orbital frequencies for the newly arrived gas that broadens the dip.

Schandl (1996) suggests that the 1.65 day dip period results from the accretion stream skimming over the surface of the disk and crashing into it at a disk radius and azimuth that vary over the 35 day cycle because of the disks warped shape. The width of the dips would most likely increase as the stream migrates closer to the disk's center, where an arbitrary surface area subtends a larger occulting angle for the compact object. The detailed shape of Schandl's model is not consistent with the inference that the stream reaches the inner accretion disk during the short high phase of the cycle, but this particular disk shape also fails to reproduce the observed X-ray and optical variability from the source. However, by adopting this type of model for the dips, it may be possible to constrain disk shape by measuring the duration of dips as a function of 35 day phase.

4. SPECTROSCOPY

The current Her X-1 model predicts that the tail of the short high state is the result of the warped disk rim gradually occulting the X-ray source as the disk precesses on the 35 day cycle (Pettersen 1977). We expect both partial-covering absorption from the tenuous upper atmosphere of the disk and opaque obscuration from the thick disk at smaller heights above the mid-disk. Similarly, dips are possibly the result of periodic increases in disk height (Crosa & Boynton 1980), absorption from the "bright spot" impact site between stream and disk (Choi et al. 1994b), or the accretion stream itself, with ejecta from the impact splashing above the disk plane (Schandl 1996). In this section we test whether the picture above is consistent with the time-varying energy spectrum of Her X-1.

A single absorber is probably unsuitable to fit a system containing an accretion disk whose density varies with vertical height and further possible absorption from winds, coronae, and magnetic accretion columns. However, the data would do a poor job constraining the large number of free parameters that a more complex fit requires. Nevertheless, we expect the partial covering model to provide a

better statistical fit than the homogeneous absorption model. We adopt a simple cutoff power-law model with cold, blanket absorption and compare this to a similar model with a partial-covering absorber.

Under the same filtering constraints as in § 3, the Standard2 events were sampled with the full pulse-height resolution of the PCA. Channels 80–255 (30–100 keV) were ignored as a result of poor counting statistics. Channels 1–6 were ignored because of uncertainties in background modeling. A cyclotron absorption feature of energy 30–40 keV is usually present in the spectrum of Her X-1 (see, e.g., Mihara et al. 1990; Dal Fiume et al. 1998). The soft wing of this feature encroaches on the PCA bandpass. Including this wing in the model provides acceptable fits, but since the center of the line is not sampled, the line parameters afford too much freedom to the low-energy components of the model. We therefore only fitted data softer than 15 keV to avoid cyclotron contamination. Cutting off the energy spectrum below 3 keV avoids soft contamination from the high-energy tails of spectral components reprocessed by the inner accretion disk. These were modeled as a 0.09 keV blackbody component and a broad Fe L emission complex at 0.95 keV by Dal Fiume et al. (1998).

An interstellar column density of $N_{\text{H,int}} = 5.1 \times 10^{19} \text{ cm}^{-2}$, consistent with the column to the source during the main high state (Dal Fiume et al. 1998), is included in the model. The effective absorption cross section $\sigma(E)$ was determined assuming neutral, solar abundance material (Balucińska-Church & McCammon 1992).

A broad Fe $K\alpha$ emission line is detected at all times except eclipse. We model this with a Gaussian of height n_{Fe} , σ -width σ_{Fe} , and spectral energy E_{Fe} . Fits to simple thermal models of iron line plus absorbed blackbody or Bremsstrahlung emission proved statistically unsuitable.

Model fitting employed XSPEC Version 10.00. We consider the spectral distribution to be a power law, with exponents fixed at its unabsorbed value, $\alpha = 0.9$ with normalization n_x , as modeled by Dal Fiume et al. (1998) and approximately consistent with the partial-covering model used for the same short high state by Oosterbroek et al. (2000). This is subject to a neutral absorber of column density N_{H} and partial covering fraction f . The composite model, $S(E)$, is represented algebraically by

$$S(E) = e^{-N_{\text{H,int}} \sigma(E)} [f e^{-N_{\text{H}} \sigma(E)} + (1 - f)] \times \left\{ n_x E^{-\alpha} + \frac{n_{\text{Fe}}}{\sqrt{2\pi\sigma_{\text{Fe}}^2}} e^{-[(E - E_{\text{Fe}})/2\sigma_{\text{Fe}}]^2} \right\}. \quad (2)$$

In our first model, where the absorbing column covers the entire X-ray source, $f = 1$ is fixed as a nonvariable parameter. In a simple scenario where we assume that the opaque structure and cool absorber are the lower and upper parts, respectively, of a disk atmosphere at an arbitrary distance from the X-ray source, the X-ray flux F_x is expected to be correlated with n_x and anticorrelated with N_{H} (and f in the partial absorption models).

Figure 3 summarizes the best-fit parameters for each visit after fitting the blanket-covering model. The power-law normalization n_x is correlated strongly with the overall flux during dips, eclipses, and "normal" states and would indicate that much of the time-dependent behavior of Her X-1 is the result of opaque obscuration rather than absorption at soft energies. The column density N_{H} is indeed anti-

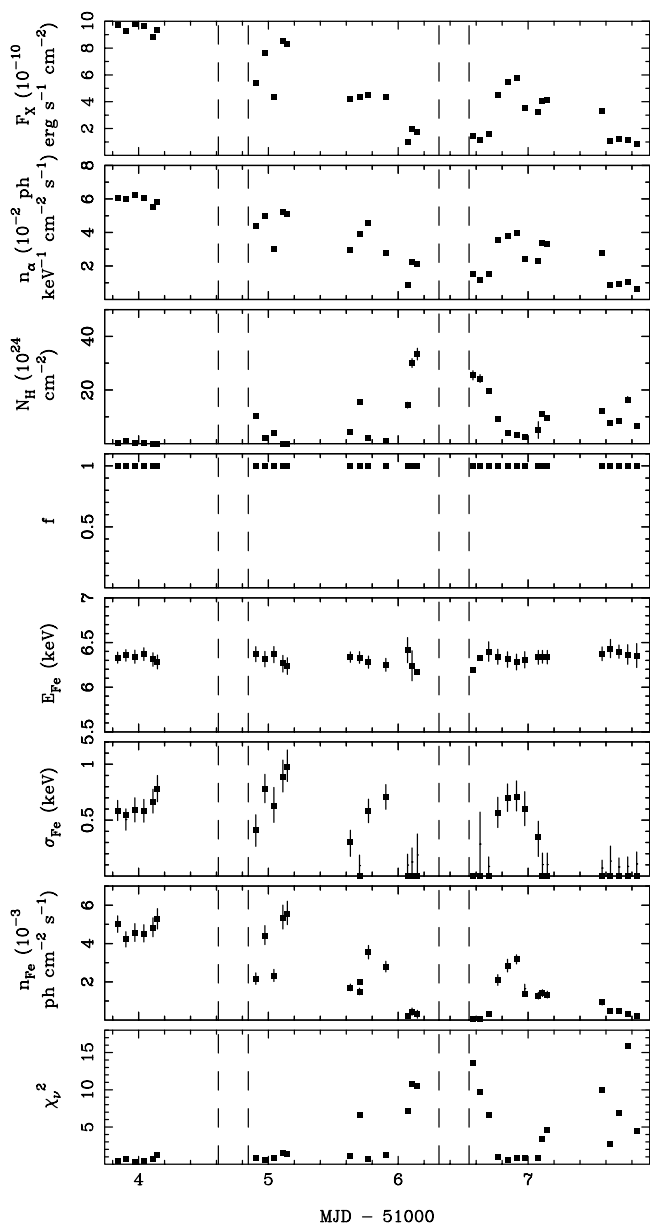


FIG. 3.—Spectral fits for each visit, where F_X is the model flux, α a power-law exponent, n_α the normalization of the power-law component, N_H a neutral absorption column density, f the partial covering fraction of the absorber, E_{Fe} the energy of the Fe K feature, σ_{Fe} the width of the Fe feature, n_{Fe} its normalization, and χ^2_v the reduced goodness-of-fit measure. Error bars are 90% confidence limits. For these fits, $f = 1$ is fixed to represent a total covering absorber.

correlated with F_X . Goodness of fits is illustrated in the lowest panel of the figure with the reduced χ^2 statistic. Fits are adequate at the peak of the short high state where there is negligible cold absorption, but their quality deteriorates during dipping events and as the high state decays. This verifies that a blanket absorber is a poor model for explaining 35 day evolution.

Figure 4 summarizes the best-fit parameters for each visit after fitting the partial-absorber model. We first note that the addition of one further free parameter, f , has improved significantly the χ^2_v from fits to dip spectra, where $\chi^2_v \sim 1$. During the peak of the high state, covering fractions are approximately 0, with column densities consistent with the

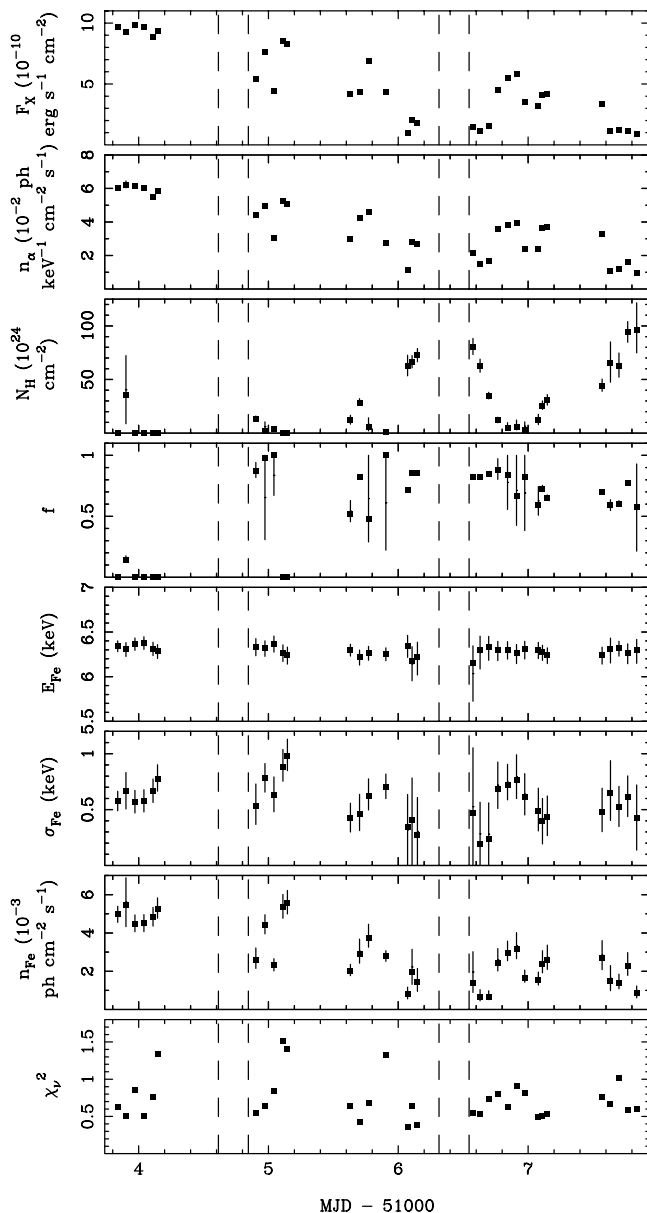


FIG. 4.—Same as Fig. 3 but for a partial-covering absorber, where f is a free parameter

interstellar value. The column density N_H is weakly correlated with f and more strongly anticorrelated with F_X and n_α . This indicates that variability in F_X is driven by both solid-body obscuration and cold, partial absorption, at least within the framework of this limited spectral model. The reality is plausibly partial or fully covered absorption by a medium of spatially varying density, as you would expect from the atmosphere of an accretion disk.

Within measurement uncertainties the energy of the Fe line is constant at 6.3 ± 0.1 keV over the duration of the pointings. This is slightly lower than the measurement of Oosterbroek et al. (2000) and Her X-1 observations in general. This could in principle result from erroneously adopting $\alpha = 0.9$. However, adopting power laws of various fixed slopes provides no energy increase and yields either identical or poorer fit quality. Additionally, allowing α freedom to vary within the fit improves χ^2_v , but the line

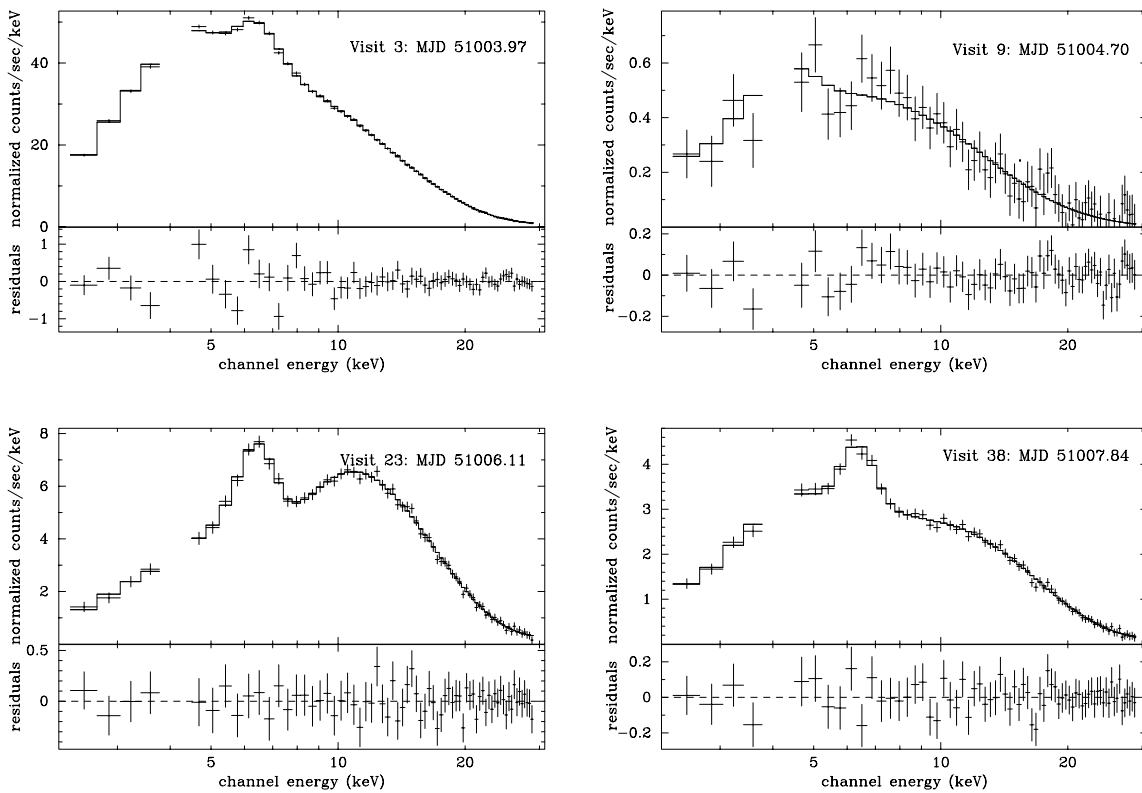


FIG. 5.—Data (crosses) and sample fits (histograms) from visits 3 (short–high-state peak intensity), 9 (X-ray eclipse), 23 (broad dip), and 38 (short–high-state tail). Residuals for each fit are in the lower panels.

energy does not increase significantly. This is identical to the model adopted by Oosterbroek et al. (2000), and there is agreement within uncertainties between $\alpha = 0.9 \pm 0.1$, $F_X = 9 \times 10^{10} \text{ ergs s}^{-1} \text{ cm}^{-2}$, $\sigma_{\text{Fe}} = 0.6 \pm 0.2 \text{ keV}$, $n_{\text{Fe}} = (2 \pm 1) \times 10^{-3} \text{ photons}^{-1} \text{ cm}^{-2}$, $f = 1 \pm 0.4$, and $N_{\text{H}} = (2 \pm 3) \times 10^{19} \text{ cm}^{-2}$ for $\chi^2_{\nu} = 0.9$

Line strength is correlated with the power-law–component normalization. This indicates that the line strength is also modulated by both 35 day effects and dip events. Dips have the same duration in both the continuum and line. The inference is that the power-law component and line have a common locality.

Residual counts remain during eclipse, which can be fitted with a single power law of $\alpha = 1.0 \pm 0.1$ and $n_x = (6.7 \pm 2.0) \times 10^{-4} \text{ photons cm}^{-2} \text{ s}^{-1} \text{ keV}^{-1}$ at 1 keV. The addition of a line component with a physically suitable energy between 6–7 keV does not improve the fit statistically. Figure 5 displays a sample of fits (the maximum and end of the short high state and both mideclipse and mid-dip).

5. PULSE AND ORBITAL EPHEMERIDES

A measurement of the pulse period at this epoch is valuable for determining the spin-down rate during the low state using future data. Figure 6 displays the neutron star spin period history of Her X-1 over the previous 30 years. The general trend is one of spin-up, but with at least two episodes of spin-down at $\sim \text{MJD } 45,000$ and $\sim 49,000$. These spin-down episodes coincide with the two anomalous low states previously reported by Parmar et al. (1985) and Vrtilik et al. (1994), respectively.

This indicates that the anomalous low states are related to a change in the location of the threading region, where gas is stripped from the accretion disk by the magnetic field of the pulsar. If the characteristic distance of this region is closer to the neutron star than the corotation radius, where the rotational velocity of the accretion disk exceeds the rotational velocity of the compact object, then assuming conservation of energy and angular momentum, the star

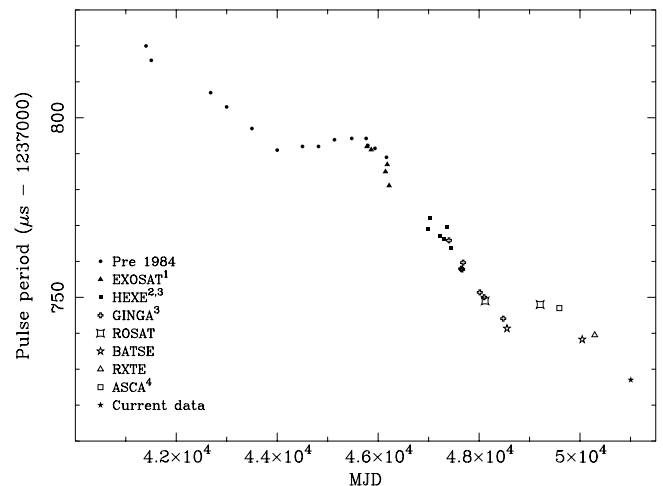


FIG. 6.—Pulse history of Her X-1. References for the observations are (1) Kahabka 1987; (2) Kunz et al. 1996; (3) Scott 1993; and (4) Stelzer et al. 1997.

will be spun up. Conversely, if the threading region occurs outside the corotation radius, we expect spin-down. Ignoring any diamagnetic properties of the accreting gas (King 1993), the location of the threading region is governed by the balance between magnetic pressure and the ram pressure of the infall. Consequently, observations of spin-down during the anomalous low states are naturally explained by a decrease in the mass transfer rate in the inner disk. Accretion does not stop altogether since UV and optical observations indicate that the companion star is still irradiated strongly by X-rays from the central object and inner disk (Vrtilek et al. 2001). The continued brightness at optical and UV wavelengths also seemingly rules out the alternative suggestion by van Kerkwijk et al. (1998) that spin-torque reversals are the result of accretion disk warp flipping the inner disk over by 180° .

Furthermore, Deeter et al. (1991) show that there is also an increase in the orbital period of the binary over time (see Fig. 7) and suggest that a broken linear expression provides a better fit to the period measurements than a continuous one. The break coincides with the low state at \sim MJD 45,000, suggesting that the anomalous low states also have a measurable effect on the orbital rate. This result is less convincing than stellar spin-up measurements and requires confirmation from orbital timing during, and after, other anomalous low states. Therefore a measurement of the orbital period at this epoch is equally useful.

For each visit, GoodXenon PCA data were reduced to light curves with a sample rate of 0.02 s over the entire detector energy response. Contemporaneous background models were subtracted and counts scaled by the number of active PCUs. Data with an elevation above the Earth's limb less than 10° or offset from the optical axis by greater than 0.02 were ignored. Visits 7–11 during X-ray eclipse were also discarded. Times were corrected to the solar system barycenter. The accuracy of the on-board clock is $100 \mu\text{s day}^{-1}$, although constant health checks adjust the clock frequency. Therefore stability on hourly timescales may be somewhat poorer.

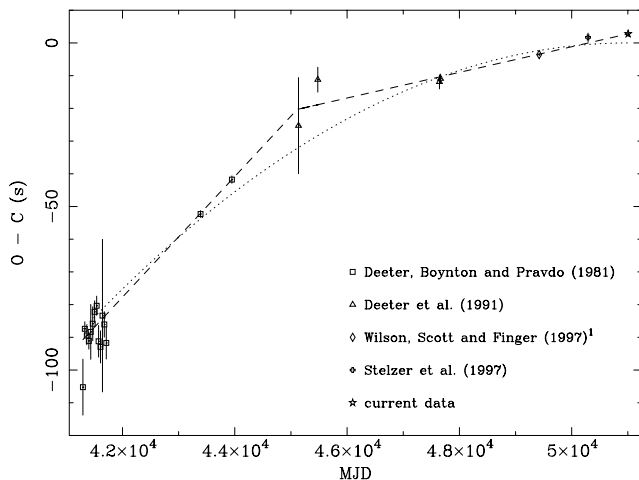


FIG. 7.—Times of superior conjunction of the neutron star minus the first two terms of the second-order polynomial fit determined in § 5. The dotted line is the quadratic term, and the discontinuous line is two linear fits broken at MJD 45,120. (1) The mean BATSE measurement between MJD 48,100 and 50,600. [See the electronic edition of the Journal for a color version of this figure.]

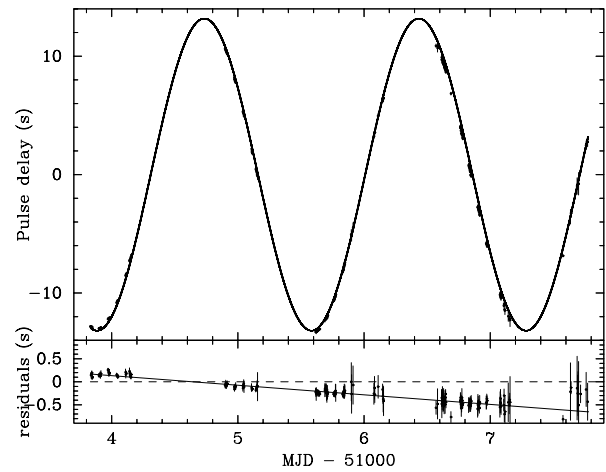


FIG. 8.—Times of pulse maximum arrival relative to the center of mass. The second-order orbital ephemeris of Stelzer et al. (1997) is overlaid on the data. Residuals plotted in the lower panel are accompanied by a linear fit. [See the electronic edition of the Journal for a color version of this figure.]

5.1. Orbital Pulse Delays

In order to measure the spin period, we must first determine time delays due to the motion of the neutron star. Data were separated into 200 s intervals and folded on a period close to the expected pulse period during this epoch, $P_{\text{spin}} = 1.237730$ s (extrapolated by eye from the BATSE timings of Wilson, Scott, & Finger 1997). A Gaussian function of pulse phase was fitted to each folded set and the centroid of each fit adopted as pulse maximum. Because of the 35 day cycle, pulse profiles vary over the duration of these visits, and consequently this method was more practical than convolving individual intervals with each other. This provided the fractional component of the orbital pulse delay. The integer component was inferred by direct comparison with the orbital fit of Stelzer et al. (1997). The orbital fit and the inferred delays are presented in Figure 8. We find a linear trend over time in the residuals where the discrepancy between the true and assumed pulse periods results in a gradient of $-0.219 \pm 0.008 \text{ s day}^{-1}$. The prediction is that Fourier analysis will reveal a pulse period of $P_{\text{spin}} = 1.2377257 \pm 0.0000004$ s after removal of pulse delays, where the uncertainty is the 90% confidence limit.

The orbital period P_{orb} was determined by minimizing χ^2 between pulse arrival times and a linear plus circular function (i.e., Still et al. 1994) and determining the phasing of neutron star superior conjunction, $T_{\pi/2}$, and pulse arrival semiamplitude, $a \sin i$. Best-fit parameters are provided in Table 1.

TABLE 1

SYSTEM PARAMETERS DETERMINED FROM THE CURRENT PULSE TIMINGS

Parameter	Value
$T_{\pi/2}$ ^a (MJD).....	51,004.729581(9)
$a \sin i$ ^b (s).....	13.1902(9)
P_{orb} (days).....	1.7002(3)
P_{spin} (s).....	1.237727(1)

^a $T_{\pi/2}$ is defined as when the mean longitude equals $\pi/2$ (i.e., superior conjunction of the neutron star).

^b The variable a is the separation of the pulsar and the binary center of mass and i the orbital inclination.

TABLE 2
BEST QUADRATIC AND LINEAR FIT PARAMETERS FOR THE ORBITAL EPHEMERIS OF HER X-1

Fit	$T_{\pi/2}$ (MJD 51,000)	P_{orb} (days)	\dot{P}_{orb} (days yr ⁻¹)	χ^2_{ν} (dof)
Quadratic.....	4.729549(7)	1.700167427(9)	$-1.33(7) \times 10^{-8}$	2.18(19)
Linear 1	4.730571(50)	1.700167790(10)	...	1.13(14)
Linear 2	4.729581(7)	1.700167504(7)	...	1.16(4)

NOTE.—The break between the two linear fits occurs at MJD 45,120.

5.2. Orbital Ephemeris

The conjunction $T_{\pi/2}$ was combined with the previous measurements of Deeter, Boynton, & Pravdo (1981), Deeter et al. (1991), Wilson et al. (1997), and Stelzer et al. (1997). We fitted these first with a second-order polynomial to determine a new orbital ephemeris, provided in Table 2, where

$$T_{\text{ecl}} = T_{\pi/2} + P_{\text{orb}} E + \frac{1}{2} P_{\text{orb}} \dot{P}_{\text{orb}} E^2, \quad (3)$$

where T_{ecl} are the times of mideclipse and E the integer orbital cycle number since $T_{\pi/2}$.

The quality of fit is slightly improved if we adopt the suggestion by Deeter et al. (1991) that the distribution is described by a broken linear expression. The corresponding ephemerides are also given in Table 2, where the break is found to occur at MJD 45,120. Both fits are overlaid on the data in the observed – computed diagram of Figure 7, where the first two terms of the quadratic ephemeris have been subtracted from data and fits.

5.3. Pulse Period

Orbital motion was removed from the filtered GoodXenon timings by subtracting a circular function of semi-amplitude $a \sin i$ and was phased by linear ephemeris 2 from Table 2. A Lomb-Scargle period search was performed over the entire sample (Press et al. 1992) and the spin period determined as $P_{\text{spin}} = 1.237727 \pm 0.000001$ s, consistent with the prediction from § 5.1. The error is the 1σ width of a Gaussian fitted to the power peak in the Lomb-Scargle statistic distribution.

Figure 6 displays the appended pulse history, where we see a general trend of spin-up, with at least two epochs of spin-down that coincide with extended X-ray low states (Vrtilek et al. 1994). We note that the first well-sampled episode of spin-down at MJD 45,000 coincides with the break between the two linear orbital ephemerides from § 5.2. The P_{spin} time derivatives during the three epochs of

spin-up were determined by linear singular value deconvolution fits and listed in Table 3.

6. PULSE PROFILES

Finally in this paper we look at the evolution of spin pulses over the short high phase. Both Deeter et al. (1998) and Scott, Leahy, and Wilson (2000; hereafter SLW) looked in detail at the profile and spectral variability of the short-high-state pulses. With this current epoch of data, we are provided with short-high-state sampling improved over those previous observations.

We filter the GoodXenon events into three energy bands: 2–5, 5–8, and 8–20 keV, remove pulse delay effects due to orbital motion (§ 5.1), and extract events from six separate time ranges (see Fig. 2): (1) MJD 51,003.8–51,004.2 (peak of the short high state); (2) MJD 51,004.7–51,004.8 (mideclipse); (3) MJD 51,004.9–51,005.2 (postclipse/predip); (4) MJD 51,006.0–51,006.6 (dip); (5) MJD 51,006.8–51,007.0 (postdip); and (6) MJD 51,007.5–51,007.9 (the endpoints of the short high state). These are presented in Figure 9. Figure 10 presents a smooth gray-scale representation of the pulses throughout the decline of the high state. In this case events have been filtered into 40 time bins and 30 phase bins. Over each time bin the mean count rate has been subtracted from the data. Bins that contain no data are represented by white horizontal strips. Figure 10 shows a small phase drift in the pulse, modulated on the orbital period with an amplitude of a few pixels. This is most likely caused by a small error (within measurement uncertainties) in the orbital time delay fit. Consequently, absolute alignment of features at different times is ambiguous, and caution is required when aligning narrow features in the pulse profile.

Using *GINGA* (Deeter et al. 1998) and *RXTE* observations, SLW developed a geometric model of the X-ray source based on the evolution of the pulse profile through the main high and short high states. Given an unobscured view of the accretion region, SLW argue that backscattering off the two magnetic accretion curtains dominates over forwardscattering. However, as the cycle proceeds, the edge of the accretion disk passes across our line of sight to the various emission regions, removing individual components from the pulse profile. SLW argue that emission from the far curtain (components B and E in their terminology) and emission from the near pole (component C) are obscured by the disk at the current 35 day phases (the far pole is never visible in the SLW model). We see no obvious signatures of components B, C, or E in the observed profiles, consistent both with this model and in agreement with the *GINGA* satellite observations of the short high state (Deeter et al. 1998).

TABLE 3
LINEAR FITS TO THE THREE EPISODES OF SPIN-UP
SHOWN IN FIGURE 6

Epoch (MJD)	\dot{P}_{spin} ($\mu\text{s yr}^{-1}$)	χ^2_{ν} (dof)
41,399–44,000.....	-3.81 ± 0.16	1.39(4)
45,761–48,552.....	-6.67 ± 0.08	1.94(22)
49,210–51,006.....	-4.35 ± 0.27	2.41(3)

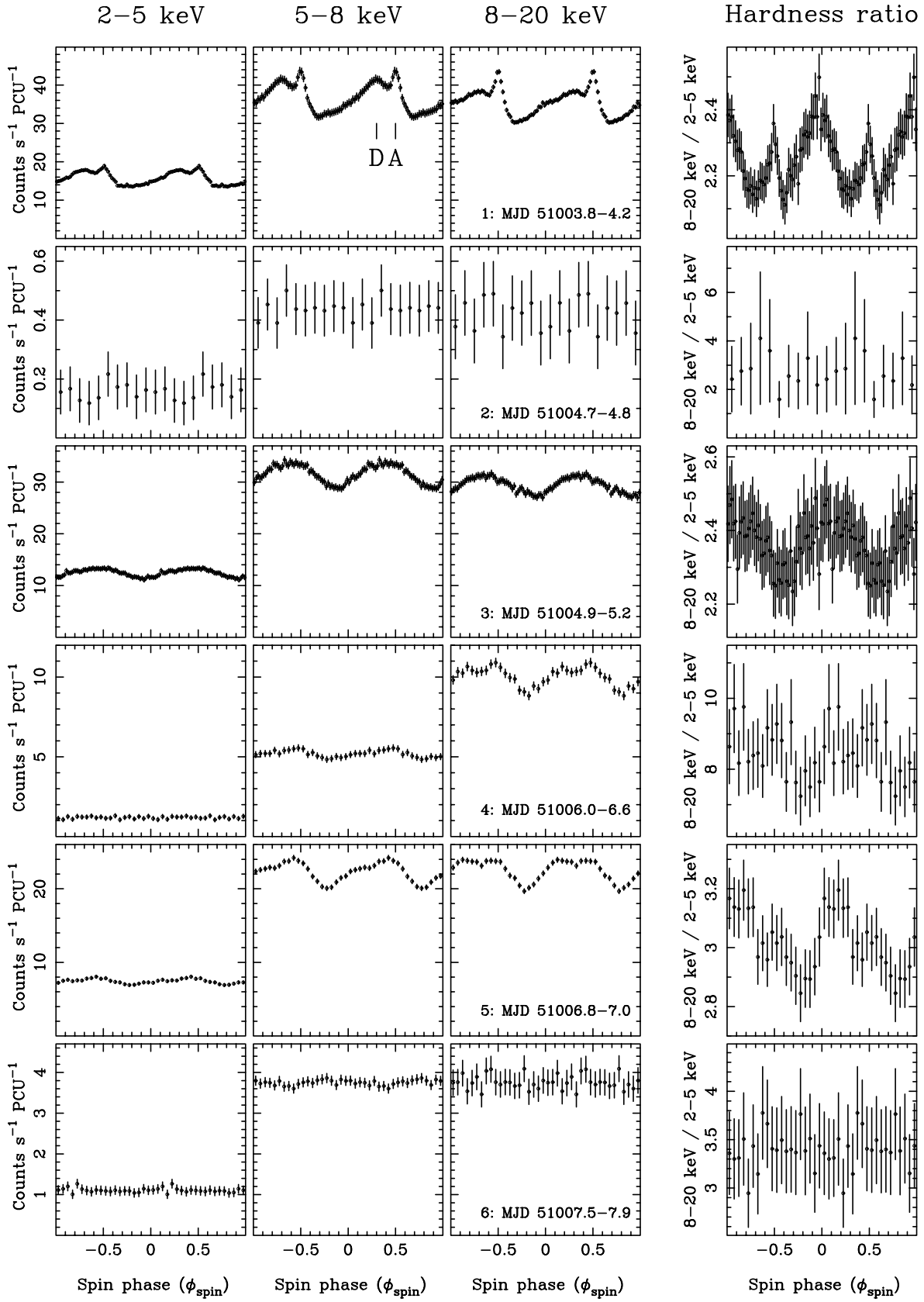


FIG. 9.—Pulse profiles sampled over six time ranges (see Fig. 2). (1) MJD 51,003.8–51,004.2 (peak of the short-high state); (2) MJD 51,004.7–51,004.8 (mid-eclipse); (3) MJD 51,004.9–51,005.2 (post-eclipse); (4) MJD 51,006.0–51,006.6 (dip); (5) MJD 51,006.8–51,007.0 (post-dip); and (6) MJD 51,007.5–51,007.9 (the endpoints of the short high state), and three energy bands: 2–5, 5–8, and 8–20 keV. “A” and “D” refer to pulse components identified by Scott et al. (2000).

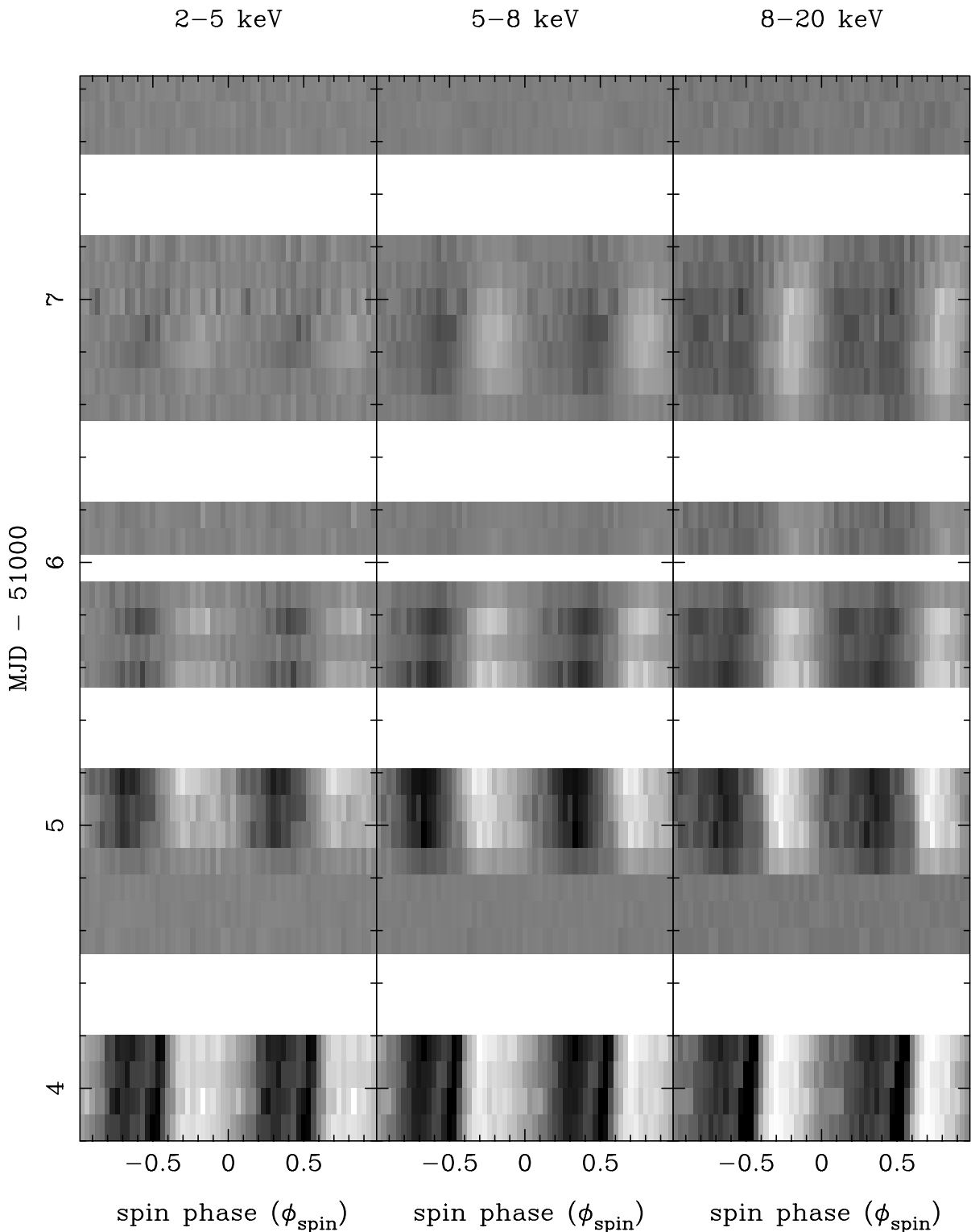


FIG. 10.—2–5, 5–8, and 8–20 keV pulses binned uniformly over time, showing the evolution of the pulse profile from the peak of the short high state to the beginning of the following low state. In each individual bin, the mean count rate has been subtracted from the data. White strips correspond to time bins with no data.

The top three profiles of Figure 9, extracted during the short–high-state maximum, are consistent with the profiles presented by SLW from a similar 35 day phase, showing a narrow peak at $\phi_{\text{spin}} = 0.5$, superimposed on a broad asymmetric modulation with a minimum at $\phi_{\text{spin}} = 0.7$ and a maximum at $\phi_{\text{spin}} = 0.3$, thus rising slower than it falls.

Between the D and A peaks is a minimum at $\phi_{\text{spin}} = 0.6$. It is reasonable to associate the narrow peak with component A, which SLW model as emission backscattered off the near curtain, close to the magnetic pole on the surface of the pulsar. We associate the broad peak with component D, which is emission from the same curtain but significantly

higher above the surface of the star. Component A is harder than component D. Component A intensity and hardness ratios are directly correlated, while component D intensity and hardness ratios do not appear to be correlated over the whole pulse cycle. The hardness ratio has a sharp maximum at $\phi_{\text{spin}} = 0.5$, corresponding to the sharp intensity peak A, and a broad roughly sinusoidal modulation peaking at $\phi_{\text{spin}} = 0.5$, halfway up the intensity rise of component D. The dip at $\phi_{\text{spin}} = 0.6$ is not accompanied by an increase in hardness ratio, as expected from photoelectric absorption.

The next row of profiles are sampled during mideclipse. During mideclipse the count rate is 100 times less than the high-state peak; however, hardness ratios are essentially unchanged, consistent with the findings of Choi et al. (1994a). Pulse fractions decrease during eclipse, and there is no compelling evidence for pulses. Consequently, the pulses are more deeply eclipsed than the mean light. The residual is thought to result from a corona surrounding the accretion disk and neutron star and/or the companion star (see, e.g., Leahy 1995).

The third set of pulse profiles has been taken from the post-eclipse recovery. In the time between the first and third pulses, component A has disappeared from the profiles. This is consistent both with the *GINGA* observations in the latter stages of the short high state and the accretion disk occulting the region responsible for this component. Component D is slightly harder than before eclipse, suggesting a higher column density in front of this region.

Set 4 of pulse profiles was extracted from the center of the next absorption dip. The hardness ratio has increased by a factor of 3 over predip pulses, expected from photoelectric absorption, and the dip at $\phi_{\text{spin}} = 0.6$ has disappeared. Here there are two peaks, at $\phi_{\text{spin}} = 0.2$ and $\phi_{\text{spin}} = 0.5$, and there is tentative evidence that both peaks are accompanied by corresponding increases in hardness. Unlike previous visits, intensity and hardness ratios are directly correlated. No pulses are detected in the 2–5 keV band.

Pulses extracted after the dip, and displayed as set 5, show a predictable decrease in hardness ratio. However, the correlation between intensity and hardness ratio remains, as do the two peaks at $\phi_{\text{spin}} = 0.2$ and $\phi_{\text{spin}} = 0.5$.

In the final set of light curves, the mean intensities are a factor 10 smaller than those in the top row, with hardness ratios indicating a larger absorption column. Evidence for pulsations is marginal however, indicating that the pulse fraction is reduced by at least a factor of 20.

The model of SLW predicts that the pulse profile should become simpler as the short high state evolves into the low state. This is the result of a number of emission regions being occulted by the disk one by one as the 35 day cycle proceeds. This is not observed. The complexity of the pulse profile increases at the tail end of the short high state. Since it is not possible for component A to reemerge from behind the accretion disk at some time during MJD 51,005.2–51,005.6, the simplest interpretation for the maximum at $\phi_{\text{spin}} = 0.5$ is that the pulse shape of component D evolves from a single asymmetric peak to a double-peaked form. Since the hardness ratios indicate no obvious photoelectric absorption event between the two peaks, perhaps the easiest way to achieve this involves a physical change in the geometry of the accretion flow. This is a reasonable solution since the location of the threading region between disk and curtain will be modified cyclically with the precession of the accretion disk.

7. CONCLUSIONS

We have presented 3–30 keV *RXTE* PCA data of what could arguably be one of the last normal short high states of the X-ray pulsar Her X-1 before it entered an anomalous low state of activity. Figure 1 illustrates that the *RXTE* ASM detected its last major main high state before the anomalous low state at MJD 51,195. There were very few (if perhaps any) short high states detected after MJD 51,004, although we note Her X-1 is a source undergoing deep eclipses and dip events, and the ASM data does not have ideal sampling. Since accretion disk structure is projected closer to the X-ray source during short high states, it is likely that the disappearance of short high states may be a precursor indicating an impending anomalous low state. We suggest that the event that caused the anomalous low state may have begun some time before it was noticed in the ASM. A study of pulse timings over this period may reveal that spin-down began (or that spin-up was decelerating) long before the high states disappeared. An interesting test to perform would be the measurement of \dot{P}_{spin} more uniformly over the epoch covered by Figure 1 using timings from the BATSE experiment that was on board the *Compton Gamma Ray Observatory* (see, e.g., Wilson et al. 1997). Comparing the current epoch PCA data with the large sample of short high states collected by the *RXTE* ASM and the limited number of previous pointed short-high-state observations by *GINGA*, we find no evidence for this particular short high state to be considered special. We have determined the orbital and pulsar spin periods at this epoch to facilitate measurements of \dot{P}_{spin} and \dot{P}_{orb} during the anomalous low and the next epoch of high-state activity.

Broadband timing verifies that the pre-eclipse dips during the short high state have durations longer than the characteristic durations of dips during main high states (Scott & Leahy 1999). It appears likely that dip durations are related to the location of the gas stream impact with the accretion disk, the trajectory of the stream, and the shape of the disk at the impact point. Detailed hydrodynamical calculations may be able to place model constraints on these properties using dip observations.

Spectrally, the short high state and the dips are consistent with obscuration of a central X-ray source by a cloud of varying column density. The standard model of a warped accretion disk of finite scale height fits this picture well.

Some modification of the recent pulse model of SLW is required to explain the evolution of pulse profiles, from relatively simple to more complex, during the tail of the short high state. We suggest (as do SLW) that geometric changes in the accretion curtains need to be considered to model the pulse profiles correctly.

This paper employed *RXTE* All Sky Monitor results made publicly available by the ASM/*RXTE* teams at MIT and the NASA Goddard Space Flight Center. This work was partially funded by NASA grants NAG 5-6711 and NAG 5-7333. K. O. B., K. H., and H. Q. acknowledge research grant support from the UK Particle Physics and Astronomy Research Council. K. H. acknowledges support from a Beatrice Tinsley Visiting Professorship at the University of Texas, Austin. We thank the referee for a thorough contribution.

REFERENCES

- Balucińska-Church, M., & McCammon, D. 1992, *ApJ*, 400, 699
- Boroson, B., Kallman, T., Vrtilek, S. D., Raymond, J., Still, M., Bautista, M., & Quaintrell, H. 2000a, *ApJ*, 529, 414
- Boroson, B., O'Brien, K., Horne, K., Kallman, T., Still, M., Boyd, P. T., Quaintrell, H., & Vrtilek, S. D. 2000b, *ApJ*, 545, 399
- Choi, C. S., Dotani, T., Nagase, F., Makino, F., Deeter, J. E., & Min, K. W. 1994a, *ApJ*, 427, 400
- Choi, C. S., Nagase, F., Makino, F., Dotani, T., & Min, K. W. 1994b, *ApJ*, 422, 799
- Crosa, L., & Boynton, P. E. 1980, *ApJ*, 235, 999
- Dal Fiume, D., et al. 1998, *A&A*, 329, L41
- Deeter, J. E., Boynton, P. E., Miyamoto, S., Kitamoto, S., Nagase, F., & Kawai, N. 1991, *ApJ*, 383, 324
- Deeter, J. E., Boynton, P. E., & Pravdo, S. H. 1981, *ApJ*, 247, 1003
- Deeter, J. E., Scott, D. M., Boynton, P. E., Miyamoto, S., Kitamoto, S., Takahama, S., & Nagase, F. 1998, *ApJ*, 502, 802
- Gerend D., & Boynton, P. E. 1976, *ApJ*, 209, 562
- Giacconi, R., Gursky, H., Kellogg, E., Levinson, R., Schreier, E., & Tananbaum, H. 1973, *ApJ*, 184, 227
- Kahabka, P. 1987, Ph.D. thesis, Technische Univ. München
- King, A. R. 1993, *MNRAS*, 261, 144
- Kunz, M., Kendziorra, E., Kretschmar, P., Maisack, M., Staubert, R., Ulmer, M. P., Kurfess, J. D., & Wilson, R. B. 1996, *A&AS*, 120, 233
- Leahy, D. A. 1995, *ApJ*, 450, 339
- Levine, A., Bradt, H., Cui, W., Jernigan, J. G., Morgan, E. H., Remillard, R., Shirey, R., & Smith, D. A. 1996, *ApJ*, 469, L33
- Middleditch, J., & Nelson, J. E. 1976, *ApJ*, 208, 567
- Mihara, T., Makishima, K., Ohashi, T., Sakao, T., & Tashiro, M. 1990, *Nature*, 346, 250
- Oosterbroek, T., Parmar, A. N., Dal Fiume, D., Orlandini, M., Santangelo, A., Del Sordo, S., & Segreto, A. 2000, *A&A*, 353, 575
- Papaloizou J. C. B., & Terquem C. 1995, *MNRAS*, 274, 987
- Parmar, A. N., Oosterbroek, T., dal Fiume, D., Orlandini, M., Santangelo, A., Segreto, A., & del Sordo, S. 1999, *A&A*, 350, L5
- Parmar, A. N., White, N. E., Barr, P., Pietsch, W., Truemper, J., Voges, W., & McKechnie, S. 1985, *Nature*, 313, 119
- Peterson, J. A. 1977, *ApJ*, 218, 783
- Press, W. H., Teukolsky, S. A., Vetterling, W. T., & Flannery, B. P. 1992, *Numerical Recipes: The Art of Scientific Computing* (2d ed.; Cambridge: Cambridge Univ. Press)
- Pringle, J. E. 1996, *MNRAS*, 281, 357
- Reynolds, A. L., & Parmar, A. N. 1995, *A&A*, 297, 747
- Reynolds, A. P., Quaintrell, H., Still, M. D., Roche, P., Chakrabarty, D., & Levine, S. E. 1997, *MNRAS*, 288, 43
- Schandl, S. 1996, *A&A*, 307, 95
- Scott, M. D. 1993, Ph.D. thesis, Univ. Washington
- Scott, D. M., & Leahy, D. A. 1999, *ApJ*, 510, 974
- Scott, D. M., Leahy, D. A., & Wilson, R. B. 2000, *ApJ*, 539, 392 (SLW)
- Shakura, N. I., Ketsaris, N. A., Prokhorov, M. E., & Postnov, K. A. 1998, *MNRAS*, 300, 992
- Stelzer, B., Staubert, R., Wilms, J., Geckeler, R. D., Gruber, D., & Rothschild, R. 1997, in *AIP Conf. Proc. 410, Proceedings of the Fourth Compton Symposium*, ed. C. D. Dermer, M. S. Strickman, & J. D. Kurfess (Woodbury: AIP), 753
- Still, M. D., Marsh, T. R., Dhillon, V. S., & Horne, K. 1994, *MNRAS*, 267, 957
- Still, M., et al. 2001, *ApJ*, in press
- Tananbaum, H., Gursky, H., Kellogg, E. M., Levinson, R., Schreier, E., & Giacconi, R. 1972, *ApJ*, 174, L143
- van Kerkwijk, M. H., Chakrabarty, D., Pringle, J. E., & Wijers, R. A. M. J. 1998, *ApJ*, 499, L27
- Vrtilek, S. D., et al. 1994, *ApJ*, 436, L9
- Vrtilek, S. D., Quaintrell, H., Boroson, B., Still, M., Fiedler, H., O'Brien, K. T., & McCray, R. 2001, *ApJ*, 549, 522
- Wilson, R. B., Scott, D. M., & Finger, M. H. 1997, in *AIP Conf. Proc. 410, Proceedings of the Fourth Compton Symposium*, ed. C. D. Dermer, M. S. Strickman, & J. D. Kurfess (Woodbury: AIP), 739
- Zhang, W., Giles, A. B., Jahoda, K., Soong, Y., Swank, J. H., & Morgan, E. H. 1993, *Proc. SPIE*, 2006, 324